Mitigating the formation of amorphous shear band in boron carbide 🄵 [SCI]

Yidi Shen, [ID] Jon Fuller, and [ID] Qi An

COLLECTIONS

🄵 This paper was selected as Featured

[SCI] This paper was selected as Scilight

View Online   Export Citation   CrossMark

ARTICLES YOU MAY BE INTERESTED IN

Cell-induced confinement effects in soft tissue mechanics
Journal of Applied Physics **129**, 140901 (2021); https://doi.org/10.1063/5.0047829

Materials for quantum technologies: Computing, information, and sensing
Journal of Applied Physics **129**, 140401 (2021); https://doi.org/10.1063/5.0050140

Axion electrodynamics in topological materials
Journal of Applied Physics **129**, 141101 (2021); https://doi.org/10.1063/5.0038804
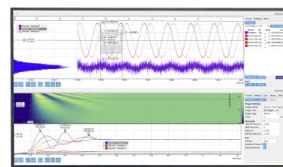
Mitigating the formation of amorphous shear band in boron carbide Ⓕ ⓢⒸⒾ

Yidi Shen, Jon Fuller, ⓘⒹ and Qi An[a] ⓘⒹ

AFFILIATIONS

Department of Chemical and Materials Engineering, University of Nevada–Reno, Reno, Nevada 89557, USA

[a]**Author to whom correspondence should be addressed**: qia@unr.edu

ABSTRACT

Boron carbide is super-strong and has many important engineering applications such as body armor and cutting tools. However, the extended applications of boron carbide have been limited by its low fracture toughness arising from anomalous brittle failure when subjected to hypervelocity impact or under high pressure. This abnormal brittle failure is directly related to the formation of a tiny amorphous shear band of 2–3 nm in width and several hundred nm in length. In this Perspective, we discuss mitigating the amorphous shear bands in boron carbide from various strategies including microalloying, grain boundary engineering, stoichiometry control, and the addition of a second phase. Combined with recent theoretical and experimental studies, we discuss strategies that can be applied in synthesizing and producing boron carbide-based materials with improved ductility by suppressing the formation of the amorphous shear band.

Published under license by AIP Publishing. https://doi.org/10.1063/5.0044526

I. INTRODUCTION

Boron carbide (B_4C) and its related materials such as boron suboxide (B_6O) have many outstanding physical and chemical properties such as low density, high hardness, chemical inertness, resistance to wear, and high neutron absorption cross section.[1,2] The combination of these excellent properties makes B_4C and related compositions potential candidates for a wide variety of engineering applications including personal body armor, abrasives, neutron capture materials,[3] and high pressure nozzles.[4] The excellent physical properties of B_4C arise from its unique crystal structure and bonding characteristics that have been measured and determined from both diffraction experiments[2,5,6] and electronic structure simulations.[7,8] The rhombohedral unit cell of the B_4C crystal, displayed in Fig. 1(a), is composed of one 12-atom icosahedron and one linear 3-atom chain that is trigonally bonded to the icosahedral clusters along the [111] rhombohedral axis or the [0001] direction of the hexagonal lattice.[2] Experimentally, it is challenging to determine the distribution of carbon atoms between the icosahedron and the linear chain because of the similar electronic and nuclear scattering cross sections of ^{11}B and ^{12}C isotopes.[6,9] Recently, our density functional theory (DFT) simulations showed that the most stable structure of B_4C is $(B_{11}C_p)CBC$, in which C_p represents the carbon on the polar site that is directly connected to another icosahedron.[8] The $(B_{11}C_p)CBC$ can also be represented as

$(B_{11}C)^{-1}$-$(C–B^+–C)$,[10] since the B in the chain transfers one extra electron to the $B_{11}C$ icosahedron, forming intra-icosahedral bonding with 26 electrons and satisfying Wade's rule.[11]

Fracture toughness is generally low in ceramics and semiconductors because it is difficult to activate mobile dislocations at low temperature due to strong covalent and ionic bonding within these materials. Particularly, B_4C exhibits anomalous brittle failure when subjected to hypervelocity impact or under high pressure,[2,12] preventing its many practical applications. This abnormal brittle failure has been extensively investigated by mechanical experiments and transmission electroscopic characterization,[12–16] as well as theoretical studies.[13,17,18] Previous experiments have shown that the brittle failure in boron carbide arises from the formation of very tiny amorphous shear bands of 2–3 nm in width and 100–300 nm in length under various loading conditions such as hypervelocity impact,[12] indentation,[13] laser shock,[14] radiation,[15] and mechanical scratching.[16] Figures 1(b)–1(d) display the transmission electron microscopy (TEM) images of the amorphous bands after B_4C is subjected to hypervelocity impact. Several theoretical studies have been performed to understand the origin of the amorphous shear bands at the atomistic level and their relationship with the abnormal brittle failure.[8,18,19] The recent DFT study focusing on the shear deformation of single crystal B_4C shows that the failure of B_4C along the most plausible slip system $(01\bar{1}\bar{1})/(\bar{1}101)$ arises from breaking the B–C bond between neighboring icosahedra, leading to
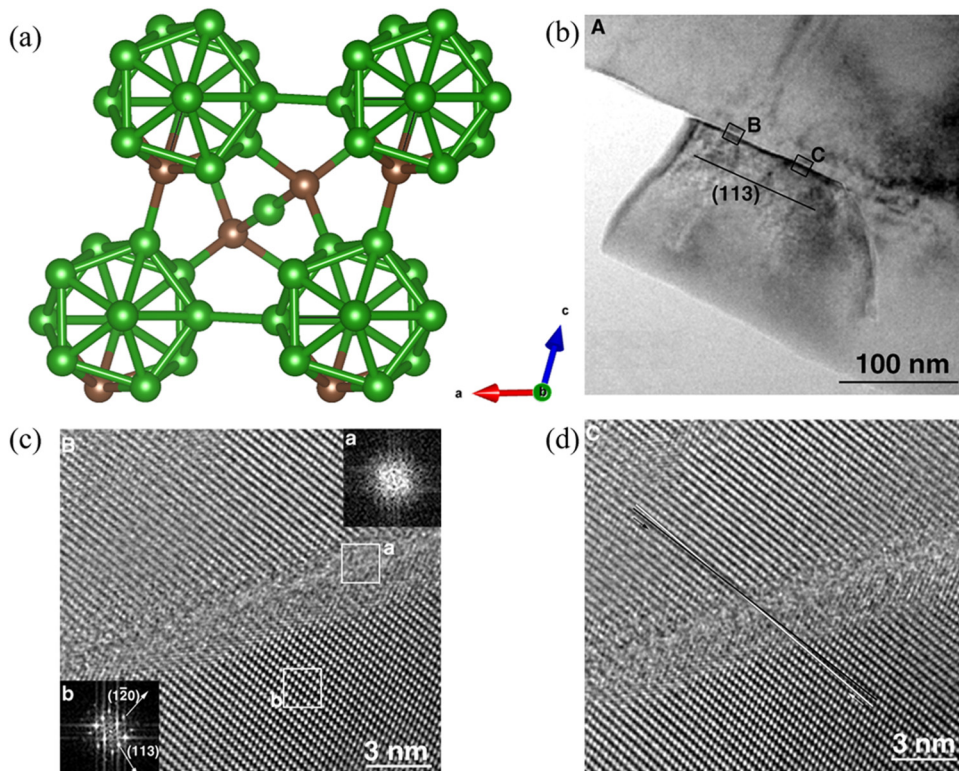
FIG. 1. (a) The crystal structure of B_4C. (b) TEM image of a planar defect originated from a corner of the fracture surface. [(c) and (d)] HRTEM images showing the localized amorphous in the region of B and C of (b), respectively. The green and brown balls in (a) represent the boron and carbon atoms, respectively. (b)–(d) are reproduced with permission from Chen *et al.*, Science **63**, 1563 (2003). Copyright 2003 The American Association for the Advancement of Science.

carbene formation.[8] This carbene then reacts with the middle boron in the chain to form a B–C bond, causing the destruction of the icosahedra and subsequent failure. However, the DFT simulations were limited to hundreds of atoms and the amorphous shear band formation was not observed directly from DFT simulations.[8] Later, reactive force field (ReaxFF) reactive dynamics (RMD) simulations were performed on the finite shear deformation of large systems (~200 000 atoms) of B_4C. In these simulations, an amorphous shear band with a width of 2–3 nm was observed within an ~20×20 nm^2 supercell, resulting in cavitation and crack opening initiating from the observed amorphous band.[18] The origin of the brittle failure is the formation of high-density amorphous bands from fractured icosahedra that favor negative pressure and cavitation.[18] This work explains the abnormal brittle failure of B_4C arising from the amorphous shear band formation, and it also suggests that the abnormal brittle failure can be suppressed by mitigating the amorphous shear band formation.[18]

B_4C and its related materials have very complex microstructural effects such as stoichiometry (B:C ratio),[20] dopants,[21] grain boundary (GB) phases, the addition of a second phase,[22] and planar defects such as twinning[23] and stacking faults.[24] The diversity provided by these microstructural considerations offers several possibilities of tuning the microstructure of the materials to suppress amorphous shear band formation and improve mechanical performance. Here we detail several strategies to mitigate the amorphous shear band formation, including microalloying, stoichiometry control, addition of a second phase, and grain boundary (GB)

engineering. Microalloying is of particular interest as a method to modify the chain structure connecting icosahedra using foreigner atoms.[10,21,25–28] Stoichiometry control can be used to modify the B/C ratio by substituting carbon with boron that results in higher shear strength and decreased amorphization.[20,29–35] The addition of second phases such as non-oxide ceramics (SiC, TiC, TiB$_2$, and C) and oxides (Al$_2$O$_3$) have also been proven to be effective in improving the mechanical properties of boron carbide.[22,36–39] Grain boundary (GB) engineering includes enhancing GB sliding to improve the ductility of nanocrystalline B_4C and the addition of dopant additives (Si) at the GBs to mitigate the amorphous shear band formation.[26,40–42]

In this perspective, we first illustrate the atomistic mechanism of forming the amorphous shear band in B_4C and then discuss various approaches that can be applied to mitigate this amorphous shear band formation. Next, we discuss the working mechanisms of these approaches through both experimental and theoretical studies. Finally, we describe the challenges in implementing these methods to the B_4C compositions and include thoughts on future improvements to these approaches for suppressing anomalous amorphous shear band formation.

II. FORMATION MECHANISM OF AMORPHOUS SHEAR BAND IN BORON CARBIDE

The damage mechanism accounting for the low fracture toughness, or the activation of an unidentified damage mechanism

in boron carbide at high impact rates and high pressures, is closely related to the formation of nanoscale amorphous bands. This was first illustrated by a classical experimental study in which high-resolution transmission electron microscopy (HRTEM) was applied to analyze the fragmentation and fracture of boron carbide under hypervelocity impact.[12] The HRTEM images of fragments showed the formation of intragranular amorphous bands with 2–3 nm width that occurs parallel to some specific crystalline planes, as shown in Figs. 1(b)–1(d). The amorphous shear bands were also observed in nanoindentation experiments,[43,44] mechanical scratching,[16,44] laser shock,[14] and under radiation,[45] suggesting that the amorphous band formation is a general mechanism of dissipating energy in boron carbide under various types of mechanical loading.

In order to illustrate the underlying mechanism behind the formation of these amorphous bands, many theoretical studies focused on the atomic structural collapse that leads to the formation of amorphous shear bands. For example, DFT simulations have been applied to examine the deformation mechanism of boron carbide under hydrostatic and uniaxial compression and concluded that the amorphous band of boron carbide arises from the reaction of bent three-atom chains with nearby icosahedra, leading to the deconstruction of boron carbide and amorphization.[35,46,47] The uniaxial compression simulations[47] showed that the C–B–C chain starts to bend with the increase in stress, as

shown in Fig. 2(a). Then, the boron atom in the three-atom chain reacts with nearby icosahedra, which prevents the recovery of the bent chain and leads to the deconstruction of B_4C.

In addition to analyzing compressive stress, scanning transmission electron microscopy (STEM) was performed in a previous nanomechanics experiment to characterize the structure of amorphous bands in B_4C.[13] It was found that the amorphous bands result from disassembly of the icosahedra during shear deformation.[13] Later, a DFT study on the shear deformation of B_4C explained the origin of amorphous band under ideal shear conditions.[8] Here, the ground state B_4C ($B_{11}C_pCBC$) is sheared along 11 plausible slip systems. The failure process along the most plausible slip system $(01\bar{1}\bar{1})/(\bar{1}101)$ contains two successive steps: first, a reactive carbene radical forms as a B–C bond connecting the two neighboring icosahedra breaks; then, this carbene reacts with the positive Lewis acidic B atom in the middle of the C–B–C chain as it moves toward the carbene during shear, leading to the disintegration of the icosahedra, as shown in Fig. 2(b).[8] Aside from this study focusing on the failure mechanism of boron carbide under ideal shear stress, we have also applied DFT simulation to investigate the structural failure of B_4C under biaxial stress that mimics complex stress condition in indentation experiments.[20] The failure mechanism is similar to that observed under the ideal shear deformation, but without the breaking of the B–C bond between
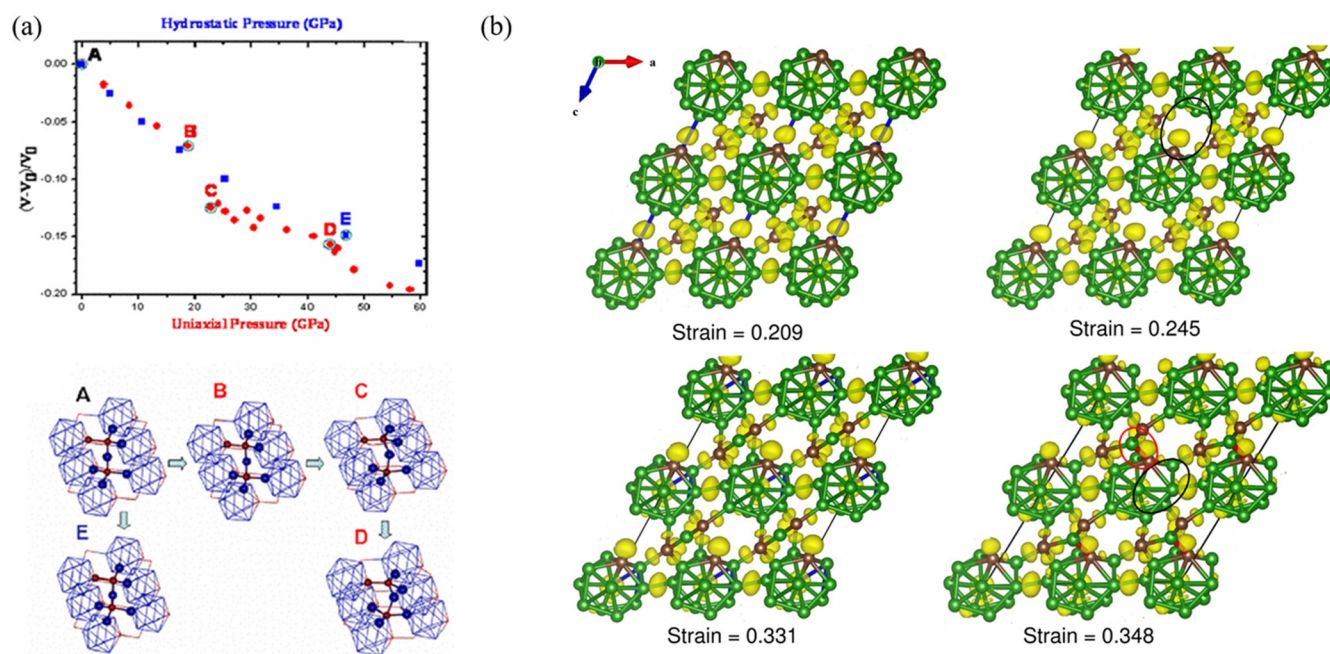

FIG. 2. (a) The upper subfigure shows the volume vs pressure of B_4C under hydrostatic and uniaxial pressures. The bottom subfigure indicates the configurations of B_4C at different stages corresponding to the points in the upper plots. From point C, the C–B–C chain starts to bend. (b) The structures and the isosurface of electron localization functional (ELF) of B_4C at different strains. At 0.245 strain, the B–C bond connecting two icosahedra breaks, leading to the formation of carbine with negative charge. At 0.348 strain, this carbine reacts with the positive Lewis acidic B atom in the middle of C–B–C chain. (a) is reproduced with permission from Yan *et al.*, Phys. Rev. Lett. **102**, 075505 (2009). Copyright 2009 American Physical Society. (b) is reproduced with permission from An *et al.*, Phys. Rev. Lett. **113**, 095501 (2014). Copyright 2014 American Physical Society.

icosahedra due to the highly compressive stress. The B^+ in the middle of the C–B–C chain reacts with the $(B_{11}C_p)^{1-}$ icosahedron, destabilizing the skeletal bonding in the icosahedron, as shown in Fig. 3.

The DFT simulations are accurate to describe the bonding conditions in B_4C and its behavior under deformation, but they are limited to hundreds of atoms, which are less than the size of the amorphous shear bands and so cannot model their behavior. Thus, in order to describe the origin of the amorphous band and illustrate the band's relationship with brittle failure, a much larger system of over 100 000 atoms are necessary. We therefore carried out large-scale (~200 000 atoms/cell) ReaxFF RMD simulations on shear deformation of B_4C.[18] In this study, we found that shear along $(0001)/(10\bar{1}0)$ slip system leads sequentially to twin formation, amorphous band formation, cavitation, and crack formation, as shown in Fig. 4. The following analysis on the RMD trajectory showed that the amorphous shear bands have a typical 5%–10% higher density than the nearby crystalline regions, leading to the tensile stress that causes cavitation and later crack opening then finally brittle failure. The higher density amorphous phase arises from the shorter B–B or B–C bonds as the icosahedra are deconstructed, which are due to the more localized bonding in amorphous B_4C phase compared to the delocalized bonding within the icosahedra for crystalline phases. The density difference between the amorphous phase and the crystalline phase increases as pressure increases, which is confirmed by DFT simulations.[18] This indicates that the brittle failure is more significant under high pressure.

III. APPROACHES TO MITIGATE THE FORMATION OF AMORPHOUS SHEAR BAND

Mitigating the amorphous shear band formation in boron carbide is the key to improving its mechanical properties such as ductility. Here, we propose several strategies to achieve this goal based on previous theoretical and experimental studies. The concepts of these strategies are illustrated in Fig. 5 and discussed below.

A. Microalloying

Microalloying has been widely used in metals to improve the mechanical properties by refining the grain microstructure or facilitating precipitation hardening. Previous theoretical and experimental studies suggest that microalloying Si into boron carbide can suppress amorphous band formation.[26] Here, we discuss the possible dopants and mechanisms to improve B_4C and related materials in this manner.

Previous studies on the failure mechanism of B_4C show that the interaction between the chain and the icosahedron plays an important role in the deconstruction of the icosahedral clusters and the formation of amorphous shear band.[8,47] This suggests that modifying the chain structures connecting icosahedra by microalloying could be an effective approach to improve the ductility of boron carbide while keeping the characteristic high hardness. Accounting for the interaction between the icosahedra in the failure process relating to the middle B atom in the C–B–C chain, a two-atom chain is preferred to suppress the deconstruction of the
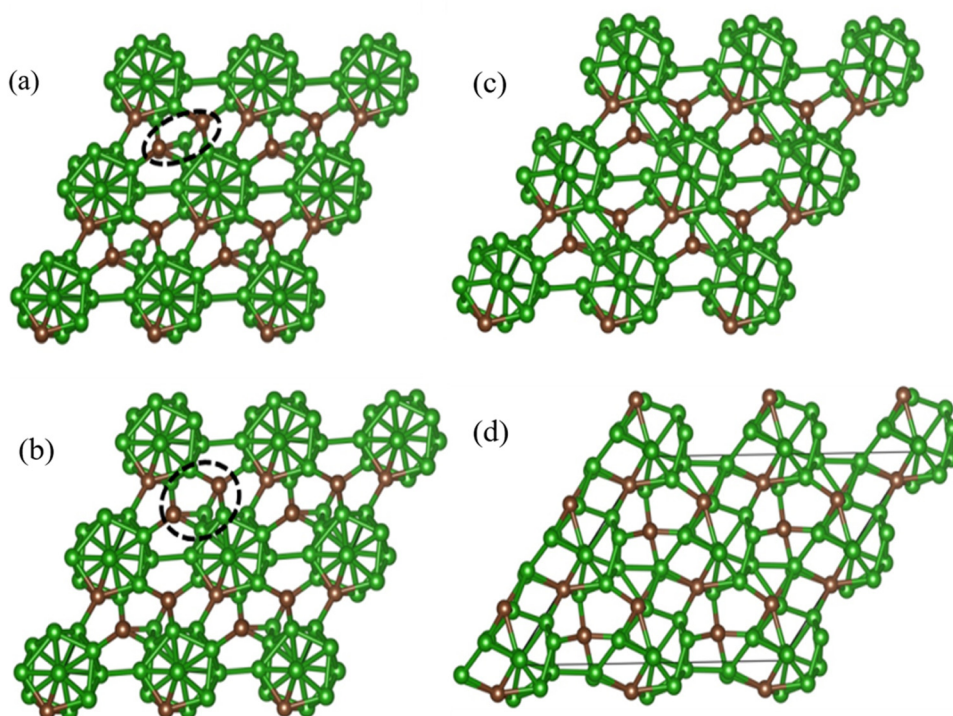

FIG. 3. The deformation and failure process of B_4C under indentation stress condition. [(a)–(c)] The B_4C structures with increased shear strain before failure in which B^+ in the C–B–C chain reacts with $(B_{11}C_p)^{1-}$ icosahedron. (d) The structure after failure. The green and brown balls represent the boron and carbon atoms, respectively. The figure is reproduced with permission from An et al., Nano Lett. **16**, 7573 (2016). Copyright 2016 American Chemical Society.
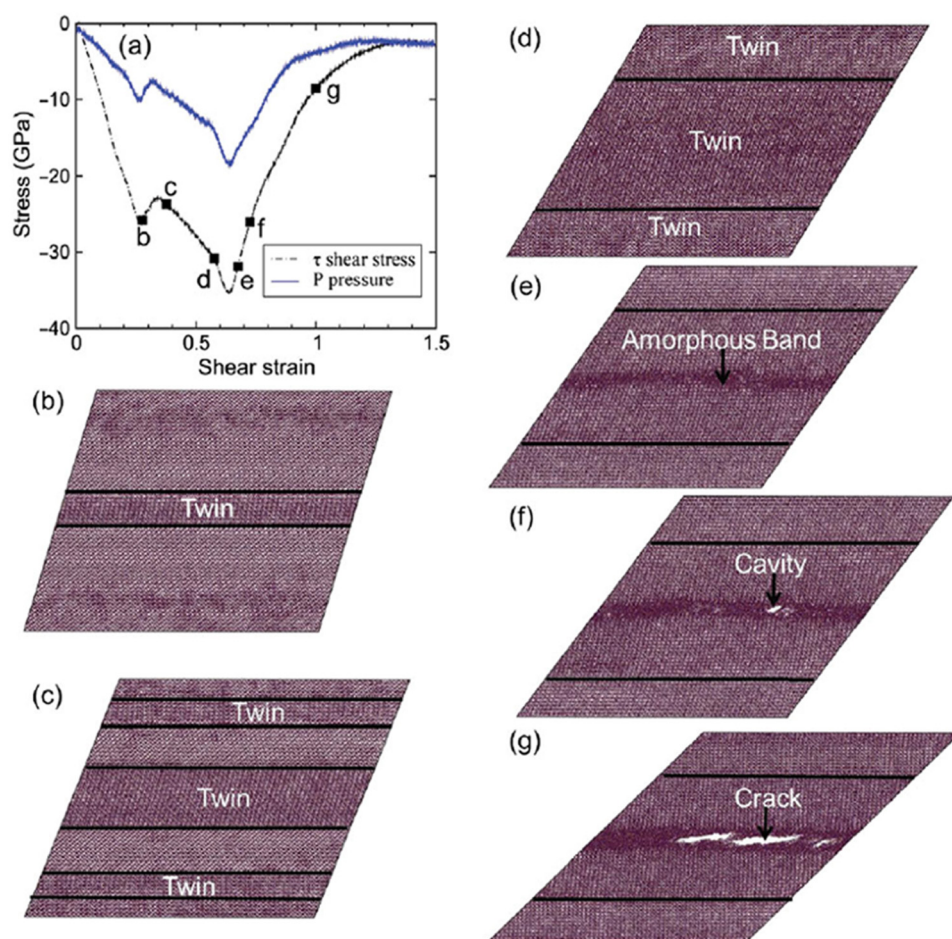
FIG. 4. (a) Stress–strain relationship and [(b)–(g)] snapshots of B_4C during shear deformation along the $(0001)/(10\bar{1}0)$ slip system. (b) Twin formation. (c) Twin growth. (d) The coalesce of twin regions across the whole cell. (e) Amorphous shear band formation. (f) Cavitation within the amorphous band. (g) Crack formation and propagation. The figure is reproduced with permission from An et al., Phys. Rev. Lett. **115**, 105501 (2015). Copyright 2015 American Physical Society.

icosahedron. A promising candidate for this is the boron subphosphide, $B_{12}P_2$, in which two phosphorus atoms form a linear chain bonded to three neighboring icosahedra.[1,48] Previous DFT simulations on the perfect crystal indicated that icosahedra in $B_{12}P_2$ do not deconstruct under both pure shear deformation and indentation stress conditions.[48] Under indentation loading, the shear stress is relaxed by the icosahedral slip between neighbor layers through breaking the P-P chain bonds.[1,48] The deformation process under indentation stress condition is shown in Fig. 6. At 0.276 and 0.514 shear strain, a P–P bond rearrangement process contributes to the release of shear stress. This leads to icosahedral slipping without fracturing icosahedra, suggesting that the P-P chain is helpful to prevent icosahedra disintegration. Another promising microalloying element is Si, which has been investigated recently. Our previous DFT simulations on the $(B_{11}C_p)Si_2$ system[27] showed that the predicted ductility index (B/G ratio from Pugh's criterion)[49] of $(B_{11}C_p)Si_2$ is larger than that of B_4C. Similar to $B_{12}P_2$, the icosahedra in $(B_{11}C_p)Si_2$ do not deconstruct under pure shear deformation. Instead, it undergoes structural transformation due to the rearrangement of Si–Si bonds, stabilizing the icosahedra from collapsing upon shearing.[27] These two studies suggest that the design

principle to modify the chain structure is to replace the three-atom C−B−C chains with two-atom chains to eliminate the highly reactive central B atom. It is worth noting that the examined slip system in both $B_{12}P_2$ and $(B_{11}C_p)Si_2$ is the same as the most plausible slip system in B_4C. But modifying the chain structure may change the most plausible slip system and future study is necessary to investigate the plausible slip systems in these two systems.

Very recently, Si was successfully incorporated into boron carbide experimentally.[50] In contrast to the Si–Si chain structure examined in the DFT simulation, the small fraction of doped Si forms a kink C–Si–C chain in Si-doped B_4C. The mechanical test on Si-doped B_4C showed that a small amount of Si doping (~1 at. %) can suppress the amorphous shear band formation. Based on the HRTEM measurement of the indentation region, the Si-doped boron carbide under indentation is dominated by short, diffuse, and multivariant shear faults, suggesting that Si doping leads to a reduction of stress-induced amorphization in boron carbide.[26] It is worth noting that the low doping concentration of Si is much lower than the theoretically proposed structures with Si–Si chain.[27] In the future, it is important to examine the phase diagram of B–C–Si under synthesis experimental conditions and
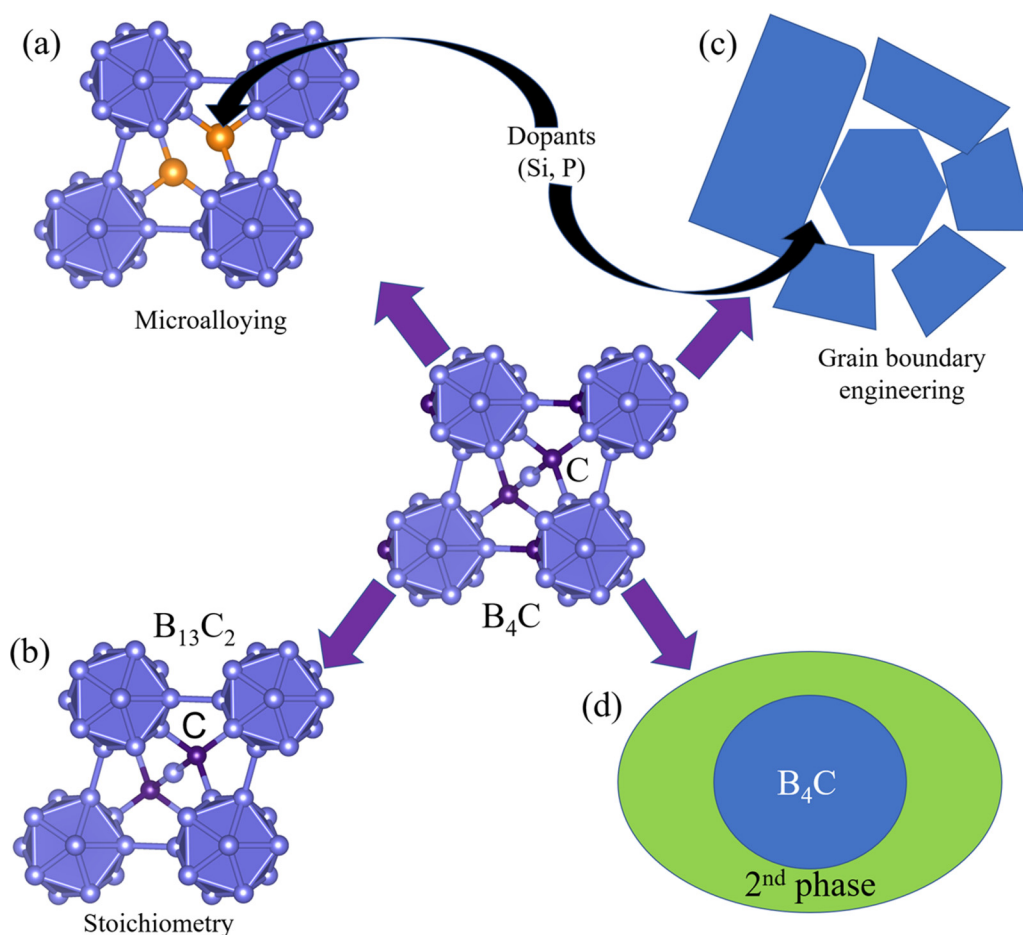
FIG. 5. The concepts of strategies to mitigate amorphous shear band formation. (a) Microalloying. (b) The structure of $B_{13}C_2$ representing the stoichiometry control. (c) The atomistic GB structure with one doped atom in the GB region. This gives an example of grain boundary engineering. (d) The addition of a second phase. The green, brown, and blue balls represent the boron, carbon, and silicon atoms, respectively.

explore possible approaches to doping a higher fractional quantity of Si into the B_4C system.

In addition to non-metal dopants, some studies have demonstrated that adding metal elements into boron carbide improves mechanical properties such as elasticity, plasticity, stiffness, hardness, and fracture toughness. These metal elements include Li, Mg, and Ti.[21,28,51–53] One recent experiment reported a newly discovered crystal structure of $Mg_3B_{50}C_8$ formed by adding molten Mg into boron-rich boron carbide ($B_{13}C_2$).[53] Later, we employed DFT simulations to examine the bonding characteristics and shear-induced failure mechanism of $Mg_3B_{50}C_8$.[21] The structural and bonding analysis suggests that the atomistic structure of $Mg_3B_{50}C_8$ can be considered two $B_{13}C_2$ supercells connecting through Mg atoms as well as icosahedral–icosahedral bonds. In addition to the strong covalent B–C bonds in $Mg_3B_{50}C_8$, the Mg atoms provide some extra electrons to stabilize the B_{12} icosahedral clusters. The calculated elastic properties of $Mg_3B_{50}C_8$ are improved compared to B_4C. Furthermore, we

found that the shear deformation and failure mechanism of $Mg_3B_{50}C_8$ are different from B_4C. The icosahedron in $Mg_3B_{50}C_8$ has not been deconstructed under pure shear deformation up to 0.833 shear strain because the B_{12} icosahedral clusters rotate to accommodate the extensive shear strain without deconstruction. For comparison, the icosahedra in B_4C are deconstructed at 0.348 strain, which results in amorphous shear band formation. These studies suggest that microalloying metal elements into boron carbide is an effective method to mitigate the amorphous shear band formation.

In addition to the toughening effects, these reported doping elements may also affect the hardness and strength of boron carbide. Previous studies showed that the doping elements do not significantly influence the hardness of boron carbide as long as the icosahedral clusters are present. For example, the theoretical study on $B_{12}P_2$ and $(B_{11}C_p)Si_2$ showed a similar hardness of $B_{12}P_2$ as B_4C, and the predicted hardness of $(B_{11}C_p)Si_2$ is slightly lower than B_4C.[27,48] Besides, a previous experiment showed that a small
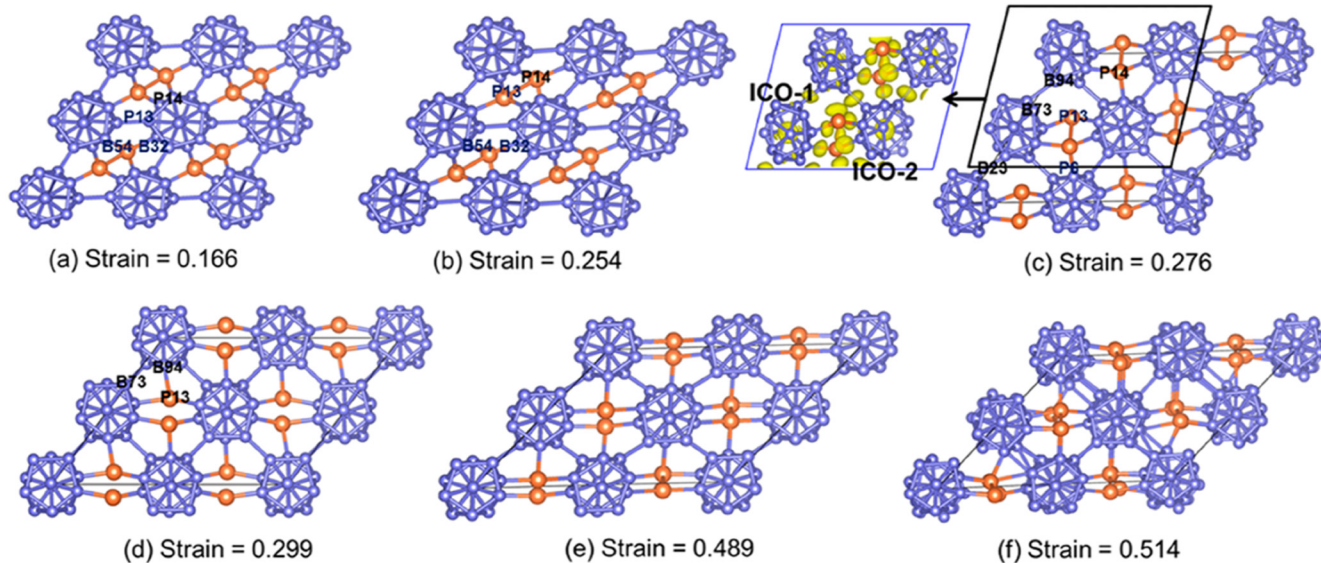
FIG. 6. The deformation and failure process of $B_{12}P_2$ under indentation condition. (a) The structure at 0.166 strain corresponding to the maximum of stress. (b) The structure before the first failure. (c) The structure after the first failure. The P13–P14 bond breaks and both of them form a new P–P bond. (d) The structure recovers the original structure. (e) The structure before the second failure. (f) The structure after the second failure. The blue and orange balls represent the B and P atoms, respectively. The figure is reproduced with permission from An *et al.*, J. Phys. Chem. C **121**, 16644 (2017). Copyright 2017 American Chemical Society.

amount of Si doping (~1 at. %) in boron carbide leads to a similar hardness as the undoped boron carbide.[50] In addition, the experimentally measured Vickers hardness (Hv) of $Mg_3B_{50}C_8$ is 32.0 GPa[53] which is higher than that of B_4C (Hv = 30.0 GPa),[54] and this is consistent with the theoretical prediction.[21] Also, the failure strength of $Mg_3B_{50}C_8$ (29.22 GPa) is slightly higher than that of B_4C (28.50 GPa) under indentation stress conditions.[21] Future research along this direction requires the combined effort of both theory and experiment. For example, it is very challenging to determine the doping sites of microalloying elements in B_4C, which have a significant influence on the deformation and failure process. Experimentally, Raman spectroscopy, x-ray diffraction (XRD), and x-ray photoelectron spectroscopy (XPS) provide effective techniques to measure the vibrational modes, the crystal structure, and the doping elements of synthesized boron carbide, respectively. To verify experimental measurements, DFT simulations can be applied to predict these spectroscopic characteristics (Raman, XRD, and XPS) with plausible atomistic structures. The comparison between theory and experiments will provide significant insight into the structural properties of doped boron carbide. In addition, the DFT simulations can be applied to characterize the doped boron carbide structure at the atomic level based on the experimental results. The enthalpy of formation of all possible structures can be calculated to determine the energetically favorable structures. After determining the favorable doped boron carbide structures, the mechanical response of the new systems can be investigated under various deformation conditions such as tension, compression, and shock to illustrate the amorphization and failure mechanisms. For realistic simulations, ReaxFF[55] RMD simulations can be applied on systems

of millions of atoms under various loading conditions. These simulations on the mechanical properties can be compared directly with mechanical experiments. For example, the theoretically predicted strength, and hardness can be compared with indentation experiments. In addition, the different levels of amorphization in the doped boron carbides from ReaxFF simulations can be compared with Raman spectroscopy and TEM measurements on the samples subjected to indentation experiments. The signature from Raman or TEM could illustrate the effects of dopants on suppressing the amorphous shear bands.

Another direction for future research is to use recently developed high throughput screening and artificial intelligence techniques to sift out the best elements (or a combination of promising elements) that can mitigate the amorphization and improve the mechanical properties. One promising approach is to apply machining learning (ML) models to analyze the effects of dopants on the mechanical properties of boron carbide and then develop an efficient strategy to sift out the promising doping elements based on these results. Recently, a strategy based on the ML model has been developed to evaluate promising doping elements to improve the magnetic performance of Sm-Co-based alloys.[56] A proper descriptor connecting mechanical properties is essential for the ML simulations, and it may be possible to build the descriptor based on the critical failure strain for the doped boron carbide.

B. The co-crystal approach

In addition to microalloying, our previous study also indicated that a co-crystal approach was a viable alternative to suppress the
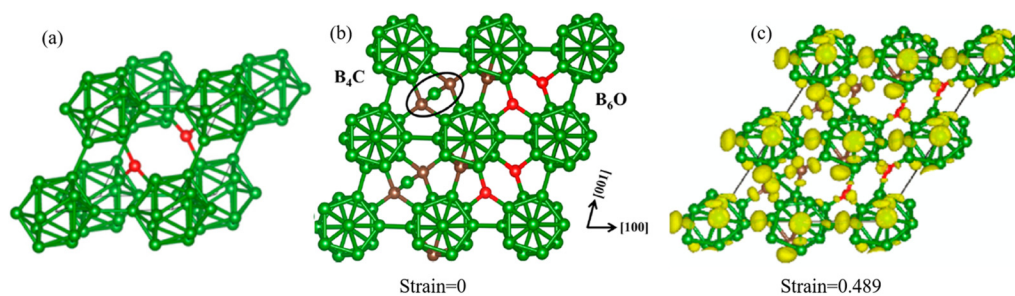
FIG. 7. (a) The crystal structure of B_6O. (b) The structure of B_4C–B_6O before shear. (c) The structure of B_4C–B_6O and isosurface of ELF analysis after failure. The B^+ in the C–B–C chain does not react with carbene. The green, brown, and red balls represent the boron, carbon, and oxygen atoms, respectively. (b) and (c) are reproduced with permission from Tang et al., J. Phys. Chem. C **119**, 24649 (2015). Copyright 2015 American Chemical Society.

amorphous shear band formation in boron carbide. Particularly, as B_4C is combined with boron suboxide (B_6O) to form a laminated structure, the failure mechanism of B_4C is suppressed under shear deformation.[10] B_6O has the same space group as B_4C.[1] The unit cell of rhombohedral B_6O (denoted as R-B_6O) consists of one B_{12} icosahedron in which six polar sites directly connect to B atoms of adjacent icosahedra while the other six equatorial sites connect with a two-atom oxygen (O-O) chain along the rhombohedral [111] direction, as shown in Fig. 7(a). Here, the chain O atom is not bonded to the other chain O atom, but is instead bonded to three nearby icosahedra.[11] The laminated co-crystal of B_6O and B_4C, shown in Fig. 7(b), was deformed under pure shear deformation and we found that this composite can undergo shear strain up to 0.465 strain without structural failure. This critical strain value is 41% higher than that of B_4C (0.331 strain).[8] The structure after failure of icosahedra at 0.489 strain is shown in Fig. 7(c). The ELF analysis on this composite structure under shear deformation suggests that the improvement of ductility arises from the presence of B_6O suppressing the interaction between the carbene and the C–B–C chain, as shown in Fig. 7(c). In addition to increased critical strain, the ideal shear strength of the cocrystal is similar to B_4C, suggesting that this laminated structure can increase the fracture toughness of boron carbide without the decrease of hardness.[10] The laminated structure has not been synthesized experimentally and it may be worthwhile to synthesize it in the future to verify these simulation results. The Raman spectroscopy and HRTEM images can be used in experiments to verify this laminated structure as well as its hardness and failure mechanism under nanoindentation conditions.

C. Stoichiometry control

The B–C system can be synthesized by different methods such as microwave carbothermal reduction of boric acid[57] or carbothermal reduction of a boric acid–citric acid gel.[58] The powders produced by these methods contain a wide range of B/C ratios resulting in different phases. Generally, boron carbide has a wide composition range from 8 to 20 at. % C, with various distributions of boron and carbon atoms into the rhombohedral crystalline lattice.[2,34,59,60] Recently, both experimental and theoretical studies have shown that this wide range of composition significantly affects the mechanical properties of boron carbide.[29,31,33,34,61] For instance, the indentation experiments on boron-rich boron carbide indicated that both the hardness and modulus of boron-rich boron carbides decrease with the increase in boron content.[29,39] A recent theoretical study showed that under uniaxial compression, the yield stress of boron carbide with higher carbon concentrations [$B_{11}C_e$(CCC) and $B_{11}C_p$(CCC)] drastically decreases compared to $B_{11}C_p$(CBC).[34] In addition, we have identified a structure of $B_{12}CBB$ with very high boron component and examined its failure process, as well as the failure process under both pure shear stress and indentation condition.[20,33] Under pure shear, both $B_{12}CBC$ and $B_{12}CBB$ have a higher shear strength than B_4C($B_{11}C_p$CBC). Under indentation conditions, $B_{12}CBC$ and $B_{12}CBB$ have similar and slightly lower ideal shear strength compared to B_4C, respectively. The findings of these studies indicated that the stoichiometries (B/C ratios) of boron carbide affect the strength of boron carbide.

More interestingly, it has been reported that a boron enrichment is helpful to mitigate amorphization in boron carbide.[30,32,62] Previous quantum mechanics (QM) simulations suggested that replacing carbon with boron in the icosahedra, which leads to the transformation of the icosahedra from $B_{11}C_p$ to B_{12}, can mitigate the amorphization.[20,34,35] This is because the transformation would prevent interactions between B in C–B–C chain and C in $B_{11}C$ icosahedron during deformation. Moreover, recent experiments showed that increasing boron concentration is favorable to mitigate the amorphization in boron carbide.[32,62] The nanoindentation experiments on two samples with different B/C ratios (B_4C and boron-rich $B_{6.3}C$)[32] showed amorphization that was quantified by the amorphous shear band densities beneath indents. The HRTEM measurements on the indented samples indicated that the amorphous bands are reduced by 30% in boron-rich $B_{6.3}C$ sample, as shown in Fig. 8(a). This finding is consistent with the Raman measurement that the amorphous peak for boron-rich $B_{6.3}C$ sample is lower than that of B_4C, as shown in Fig. 8(b). In addition to the reduction of amorphization, the measured hardness of $B_{6.3}C$ shows a small drop (~4%) compared to B_4C, which may be induced by standard errors from experiments.[62]

These theoretical and experimental findings suggest that stoichiometry (B/C ratio) control is an effective approach for
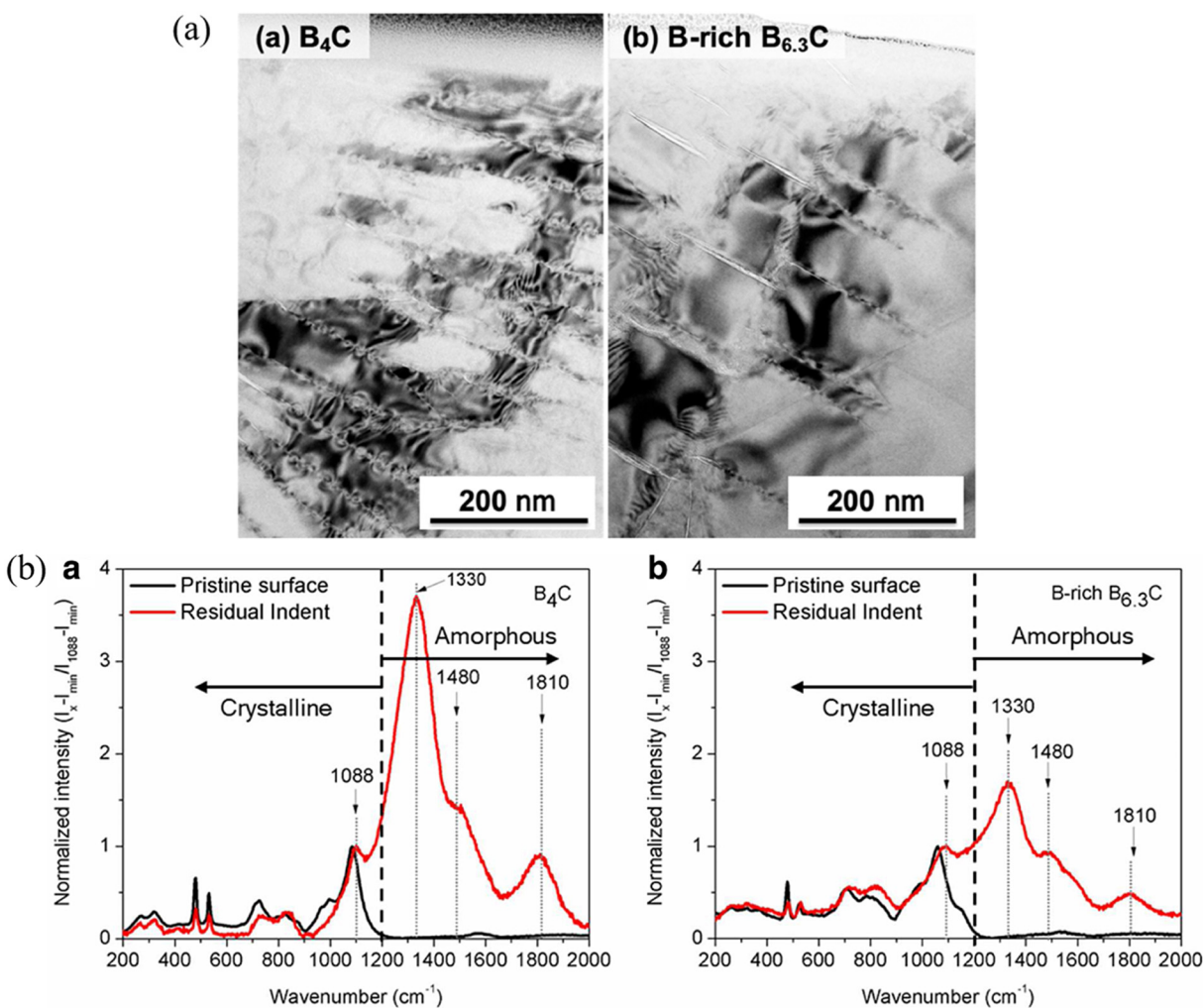
FIG. 8. (a) The HRTEM images of B_4C and $B_{6.3}C$ under indentation loading. The number of amorphous bands in B_4C is higher compared to $B_{6.3}C$. (b) The Raman spectra from the indented region of B_4C and $B_{6.3}C$. The peak of amorphous phases in B_4C is higher than the peak in $B_{6.3}C$. The figure is reproduced with permission from Chauhan *et al.*, Acta Mater. **181**, 207 (2019). Copyright 2019 Elsevier.

mitigating the amorphous shear band formation in boron carbide. In addition, boron and carbon atoms are similar in size, making it relatively straightforward to substitute one with the other to form many possible stable and energetically favorable structures. However, it remains challenging to identify both the detailed atomic structures and the distributions of B and C atoms in these complex phases. For example, some studies suggested that the boron atom is favored to substitute the carbon atom in the chain[29] while others indicated that the boron atom replaces the icosahedral carbon.[39] Therefore, it is important to correctly identify the stable structure of boron-rich boron carbide. Experimental samples may include various configurations such as $(B_{12})CBC$, $(B_{11}C_p)CBC$, and $(B_{12})CCC$; simulating this system is therefore beyond the capacity of QM methods. To solve this problem, it is thus important to

simulate the mixed configurations with a force field that can describe the energetics of various phases and configurations accurately. A well-developed ReaxFF will be suitable for this kind of simulation.

D. Grain boundary engineering

Grain boundaries (GBs) play an important role in the mechanical properties of metals and ceramics and have been studied extensively for metals and alloys.[63,64] GBs have been observed from TEM measurements in boron carbide, like other covalent solids.[39,65] However, the presence of GBs weakens the strength of icosahedra next to GB, leading to the initialization of amorphization.[66] In order to understand the failure mechanisms

arising from GBs, we applied QM simulations to investigate the mechanical response of B_4C with GBs under both pure shear and biaxial shear deformation that mimics indentation stress conditions.[66] In this study, we examined two specific GB models including (1) GB-I rhombohedral $(111)/(\bar{1}\bar{1}3)$ in which integral icosahedral clusters are along GBs and (2) GB-II $(2\bar{1}\bar{1})/(\bar{2}11)$ in which the deconstructed icosahedral clusters are along GBs. We found that the GB model has a much lower critical shear strength than the single crystalline B_4C, suggesting that the mechanical failure would initiate from GB regions in polycrystalline B_4C. In addition, it is critical to design high-energy GBs in boron carbide to facilitate the GB sliding so that the ductility can be improved. Here, we propose two approaches to modify the GB properties so that the amorphous band formation can be prevented via grain boundary engineering: decreasing grain sizes and doping additive elements at the GBs.

1. Grain size effect

Grain boundaries (GBs) act as obstacles for mobile dislocations in polycrystalline metals,[63,67] leading to increased strengths as the grain size decreases to approximately 20–30 nm, known as Hall–Petch relationship.[68,69] The Hall–Petch relationship breaks down at small grain size as grain boundary sliding becomes dominant. In nanocrystalline ceramics such as SiC and $MgAl_2O_4$, this relationship is also observed experimentally.[70,71] In particular, the Hall–Petch relationship breaks down as the grain size decreases to ~20 nm in $MgAl_2O_4$. However, GBs play a quite different role in the deformation and failure mechanisms of ceramics as compared to metals. Thus, it is crucial to investigate the relationship between grain size, grain sliding, ductility, and strength in GB structures of boron carbide.

We combined ReaxFF RMD simulations and experimental TEM measurements to investigate the GB sliding for multiple grain systems with grain sizes ranging from 5 to 15 nm.[40] Particularly, in RMD simulations, we constructed three nanocrystalline B_4C (n-B_4C) models with different GB structures and examined the finite shear deformations of three models of n-B_4C at room temperature. We found that the ideal strength of n-B_4C decreases as grain size decreases, as shown in Figs. 9(a) and 9(b), suggesting that the hardness of n-B_4C tends to be lower with smaller grain size. However, from stress–strain relationship [Fig. 9(a)] and failure
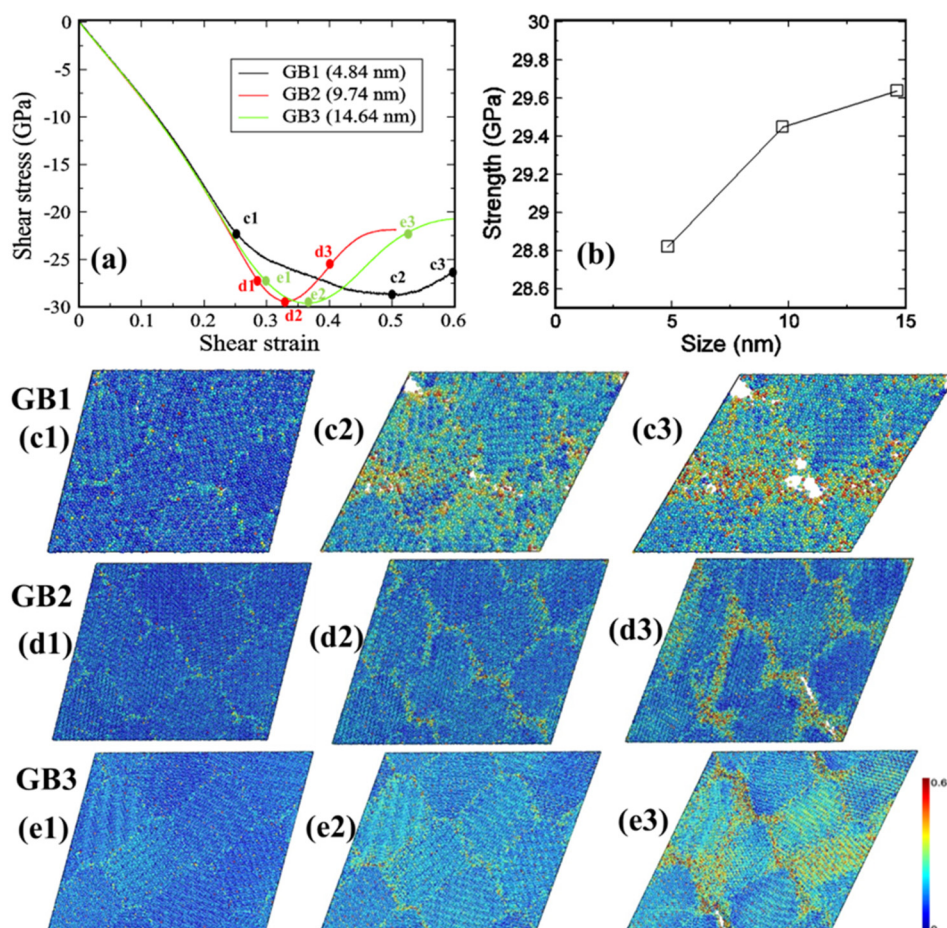

FIG. 9. (a) The shear-stress–shear-strain relationships of n-B_4C with three grain sizes under ideal shear deformation. (b) The ideal strength vs grain sizes. [(c)–(e)] The snapshots for three GB models at different stress corresponding to the points in (a). [(c1)–(e1)] The snapshots of the beginning of plastic deformation. [(c2)–(e2)] The snapshots with maximum shear stress. [(c3)–(e3)] The snapshots of formation of cavitation. The figure is reproduced with permission from Guo et al., Phys. Rev. Lett. **121**, 145504 (2018). Copyright 2018 American Physical Society.

process [Figs. 9(c), 9(d), and 9(e)], we found that the amorphization initiates at 0.5 strain for the GB1 model with 5-nm grain size, which is higher than the critical strain of the other two GB models. This is due to the high-energy GB development under shear deformation, which agrees with the previous QM results.[66] In addition, the dominant deformation mechanism of the plastic deformation process is GB sliding, which facilitates the intergranular fracture rather than the transgranular fracture. This deformation mechanism in n-B_4C is also verified by TEM observations. This study suggests that high-energy GBs can significantly promote the plastic deformation, postpone the amorphization, and enhance the fracture toughness of microsize B_4C. This indicates that a critical design consideration for mitigating the amorphous band formation is to decrease the grain size to the nanoscale.

2. Doping additive elements at the GBs

Another approach to preventing amorphization near the GBs of boron carbide is to modify the chemistry of the GBs by adding dopants in GB regions that increase the GB energy. Some suitable dopants for this purpose including Al and Si were successfully added into GBs experimentally.[42,72–74] Al is one of the preferred candidates for the development of B_4C cermets because it is a stable metal with a low specific gravity.[72,73] It is also ductile, nontoxic, relatively inexpensive, easy to obtain, and available in corrosion-resistant forms. Combining Al with B_4C forms the boron carbide–aluminum cermet that exhibits both high hardness and toughness in a lightweight structure. In addition to boron carbide–aluminum composite, adding a small amount of Al into the boron carbide leads the distribution of Al into the GB regions.[42,74] The XRD and SEM analyses indicated that as Al is added in the pressureless sintering process of B_4C at 2050 and 2150 °C,[74] the added Al forms AlB_2 and Al_3BC in the GB regions. In addition, a very recent experimental study elucidated the effect of some oxide additives including Al_2O_3, SiO_2, and B_2O_3 on the structure and chemistry of GBs of boron carbide.[42] The EDS analysis indicated that the GB exhibited excess concentrations of Si and Al, suggesting that both Si and Al can be absorbed by the GB regions and modify the chemistry of the GBs.

Si and Al appear to be promising candidates for the GB engineering required for preventing amorphization at the GBs. In the future, it is essential to examine their effects on the mechanical properties of nanocrystalline B_4C, such as changes in hardness, strength, and fracture resistance. The doped Si in GB regions may help prevent the disintegration of icosahedra near GBs and thus mitigate the amorphous shear band formation arising from GB regions. Therefore, it is important to examine the concentration of Si in GB regions from experiments and requires future mechanical experiments examining the Si-doped polycrystalline B_4C systems. HRTEM is very important for analyzing the underlying deformation mechanism of the Si-doped B_4C at the atomic level. The theoretical studies employing DFT and MD simulations are likewise very important for determining the distribution of Si in GB regions, as well as illustrating the deformation and failure mechanism of GB-doped system under various loading conditions. To accurately describe the GB properties, it is important to train

ReaxFF parameters based on QM simulations to reproduce the energetics and structures of various GBs.

E. Addition of the second phase

In commercial boron carbide samples, some additives, such as carbon,[39] TiC,[38] SiC,[75] TiB_2,[76] and Al_2O_3,[77] are added to facilitate the sintering and densification of boron carbide. These additives act as a second phase in the system and also affect the mechanical properties of boron carbide.[39,77,78] For example, the addition of Al_2O_3 into boron carbide improves the fracture toughness but also reduces the hardness due to the low hardness of Al_2O_3.[22,77,79,80] Another example is adding free carbon in boron carbide to inhibit grain growth, leading to relatively fine microstructures. However, it was reported that the carbon additives also reduce the hardness of boron carbide and its effect on toughness is controversial. The carbon in boron carbide has a toughening effect associated with crack deflection[81,82] while it can also act as a crack nucleation site which reduces the fracture toughness and result in microcracking in the neighboring grains.[39] These controversial effects might arise from the different size, distributions, and added concentrations in the different boron carbide samples.[39]

The common second phases in boron carbide are the SiC and TiB_2 phases synthesized by reactive hot pressing with different starting materials.[75,76] Both SiC and TiB_2 exhibit good mechanical and chemical properties, such as high hardness, good chemical stability, and high oxidation resistance.[83] Thus, they have been used as additives not only to keep the relatively high hardness but also to improve the fracture toughness of boron carbide.[75,76] The experimentally synthesized B_4C–SiC nanocomposite could be achieved through mechanochemical processing with B_4C, Si, and graphite powders and subsequent hot pressing (sintering temperature: 1700–1900 °C).[75] The fracture toughness of this composite synthesized at 1900 °C is 6.1 MPa m$^{1/2}$, which is higher than that of B_4C^2. This improvement in fracture toughness arises from fracture deflection, and the mechanism of which is attributed to the presence of intergranular fracture at the intracrystalline boundary between intragranular particles (SiC particles) and B_4C matrix, as shown in Fig. 10(a). When cracks cross the B_4C grains and reach the intracrystalline boundary, the cracks cannot cross the intragranular particles but instead are deflected along the intracrystalline boundary due to the small-size and high-strength intragranular crystals while consuming crack extension energy, as shown in Fig. 10(b). Also, the Vickers hardness of this composite is 30.1 GPa, which is comparable with pure B_4C, suggesting that adding SiC in B_4C can enhance the overall toughness of the B_4C–SiC composite and keep the high hardness. In another study, the B_4C–20 mol. % TiB_2 ceramic composites were successfully fabricated by reaction hot pressing at 2000 °C.[84] This composite possesses both high hardness of 866 MPa and improved fracture toughness of 3.2 MPa m$^{1/2}$. In order to further improve the fracture toughness of B_4C ceramics, the B_4C–TiB_2–SiC triple-phase composite was synthesized by adding both TiB_2 and SiC into B_4C. In addition, the B_4C–TiB_2–SiC triple-phase composite can also be fabricated via reactive hot-pressing sintering (1850 °C) using B_4C and 30 vol. % nanolayered Ti_3SiC_2, and the composite has the high micro-hardness and fracture toughness of 31.6 GPa and 8.0 MPa m$^{1/2}$, respectively.[84] Its
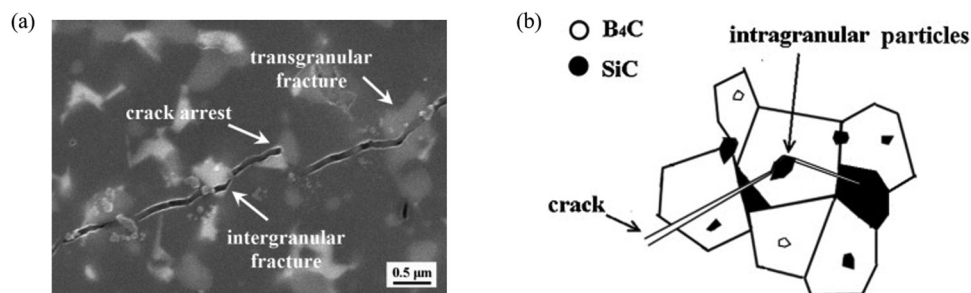
FIG. 10. (a) The SEM image of the B_4C–SiC sample with both intergranular and transgranular fractures. (b) The mechanism of crack deflection in the intergranular and transgranular composites. The figure is reproduced with permission from Zhang *et al.*, J. Eur. Ceram. Soc. **34**, 2153 (2014). Copyright 2014 Elsevier.

high hardness is due to the low open porosity and grain refinement, while the high toughness arises from fracture deflection in the intracrystalline boundary between intragranular particles (TiB_2 and SiC) and the B_4C matrix that initiates intergranular fracture and consumes more crack extension energy similar to the behavior of the B_4C–SiC composite.

Despite these experimental studies on synthesizing B_4C based composite materials with improved mechanical properties, the understanding of the effect of these second phases on the deformation and failure mechanism remains limited. Under realistic conditions, the deformation mechanisms and threshold stress of amorphization could drastically change. Thus, it is important to investigate the effects of the second phases on both of them. For example, more experiments can apply some loading tests to examine the deformation and failure mechanism of the boron carbide with second phases and then compare to the behavior of pure boron carbide. TEM measurement can also be applied to directly observe the deformation mechanism at the atomic level. In addition, some electronic and atomistic level simulations (DFT and MD) can be performed to understand the deformation mechanism of boron carbide with second phases. The obtained results can be combined with mesoscale and continuum models to simulate the fracture/fragmentation in boron carbide with second phases under realistic conditions.

IV. MATERIALS BY DESIGN THROUGH GRAIN BOUNDARY ENGINEERING

In Sec. III, we discussed possible design strategies to improve the mechanical properties of boron carbide under realistic conditions, resulting in the mitigation of amorphous shear band formation and improved ductility. Out of all these approaches, grain boundary engineering using additives is the most promising and worthy of being discussed separately because of the ubiquitous GB structures in ceramics. But the studies on GB engineering of boron carbide are limited because of the complexity of GB structures and local chemistry as additives are added to GBs. In contrast, for other structural ceramics such as Si_3N_4, SiC, and $SrTiO_3$, several microstructural engineering approaches have been developed and applied to improve their fracture resistance through extrinsic mechanisms, such as phase transformations, microcracking, crack-deflection, and crack-bridging.[85–87] For example, for Si_3N_4, the mechanism of toughening arises from amorphous intergranular films (AIFs) within GBs.[87] These grain boundary amorphous films weaken grain boundaries, making intergranular fracture rather than transgranular fracture favorable in Si_3N_4. Owing to

increased path length for the crack, the fracture toughness is increased. For boron carbide, it has sharp and clean GBs that lead to transgranular fracture. In addition, these GBs weaken the strength of the $B_{11}C$ cages, leading to the initiation of amorphization. Therefore, modifying the chemistry or structure of GBs in boron carbide can be a very important step to improve the mechanical properties of boron carbide under realistic conditions.

There are two approaches to GB engineering for boron carbide. First, the proper design of GB structures by adding suitable dopants is helpful to mitigate the amorphous shear band formation initiated by deconstructing $B_{11}C$ icosahedra next to the GBs, as discussed in Sec. III. Out of all dopants, Si prevents the disintegration of icosahedra near GBs the best and thus mitigates the amorphous shear band formation arising from GB regions. Second, AIFs might also be formed by using some additives in GBs, leading to a transformation of the favored fracture mechanism from transgranular fracture to intergranular fracture, which can improve the fracture toughness in boron carbide. Following these design strategies, both theoretical and experimental studies can be combined to examine grain boundary engineering to improve the mechanical properties of boron carbide. For instance, future experiments could include variations of grain boundary chemistry, variations of grain boundary structure, and additive synthesis. In future theoretical studies, the QM simulations can be applied to characterize the GB structure before and after adding dopants at the atomistic level. However, the GB structures in boron carbide are very complex, making it a challenge to construct many plausible GB structures. For GB engineering, it is important to develop practical approaches to construct the atomistic GB models. Recently, several promising methods have been proposed to construct interfacial or GB structures of various materials from first-principles.[88–91] In this approach, possible GB structures are generated by inserting and removing atoms from GB core and changing GB dimensions as well. The energies of all generated structures are calculated using empirical force fields so that the low-energy configurations can be sifted out and automatically stored. After that, a clustering procedure is designed to group each possible configuration based on the thermodynamic and crystal symmetry information. This approach can also be applied to search possible GB structures in boron carbide with an accurate force field. The predicted GB structures can be validated by TEM measurements. The deformation mechanisms of these GB structures under various loadings can also be predicted by QM simulations so that the effects of modified GBs on the mechanical properties of boron carbide can be revealed. Furthermore, a ReaxFF method can be developed based on the QM simulations and then large-scale RMD simulations can be

performed to investigate stress–strain relations, the stress threshold for amorphization, the deformation mechanisms, and crack initiation in the models with modified GBs.

In addition to the QM and RMD simulations at the atomistic level, it will be useful to apply a recently developed approach, atomistic field theory (AFT),[92,93] to examine the distributions of dopants in different GB regions of nanocrystalline boron carbide and how these dopants affect the overall toughness of boron carbide. The principle of AFT is the two-level structural description of crystals such as the Bravais lattice (crystal = lattice + discrete atoms).[93] Thus, the physical properties of a multiatom system can be expressed as a formalism with a homogeneous and continuous function in space at the cell level and a noncontinuous and inhomogeneous function within the lattice cell at the substructural level.[92] In particular, the atomic deformation of a material consists of two terms including the continuous lattice deformation and discrete internal deformation.[94] This approach has been applied previously to examine the boron, boron/nitrogen, and silicon/nitrogen-doped nanocrystalline silicon carbide (SiC) models.[94]

V. CONCLUSION

In summary, we reviewed and discussed the various strategies to improve the mechanical properties of super-hard boron carbide that exhibits abnormal brittle failure when subjected to hypervelocity impact or under high pressure. This brittle failure arises from the formation of an amorphous shear band due to the deconstruction of icosahedra. Therefore, it is important to inhibit the formation of the amorphous shear band. From this perspective, we first discussed the detailed mechanism of amorphous shear band formation based on previous experimental and theoretical studies. Next, we proposed several approaches to mitigating the amorphous shear band formation, including microalloying, stoichiometry control, grain boundary (GB) engineering, and the addition of a second phase based on the microstructure in boron carbide. For each approach, we discussed the recent progress that provides guidance to suppress the amorphous band formation. We also discussed the remaining problems and potential methods that can be used to solve these issues in a future study.

We first discussed the microalloying approach including alloying proper elements such as non-metal elements, Si and P, and metal elements, Mg and Li. Then, we reviewed the co-crystal approach of combining B_4C with B_6O to form a laminated structure. We next discussed employing stoichiometry control using boron enrichment to mitigate amorphization in boron carbide and the addition of SiC and TiB_2 as a second phase to improve the fracture toughness of boron carbide. Finally, for grain boundary (GB) engineering, we discussed the strategy of controlling grain sizes that leads to the promotion of the plastic deformation in nanocrystalline boron carbide. In addition, several additives in GBs that can modify the GB chemistry and structure provide another promising GB engineering approach to suppress the amorphization arising from GBs.

It is worth noting that GB engineering using additives is the most promising among all strategies discussed herein. Therefore, we proposed two research directions along with this approach: (1) amorphous intergranular films that could be formed by using some additives in GBs, which can improve the fracture toughness in

boron carbide; and (2) the proper design of GB structures that is helpful to mitigate the amorphous shear band formation initiated by deconstructing $B_{11}C$ cages next to the GBs.

DATA AVAILABILITY

The data that support the findings of this study are available from the corresponding author upon reasonable request.

REFERENCES

[1]Q. An and W. A. Goddard, Chem. Mater. **27**, 2855 (2015).
[2]V. Domnich, S. Reynaud, R. A. Haber, and M. Chhowalla, J. Am. Ceram. Soc. **94**, 3605 (2011).
[3]A. N. Caruso, P. A. Dowben, S. Balkir, N. Schemm, K. Osberg, R. W. Fairchild, O. B. Flores, S. Balaz, A. D. Harken, B. W. Robertson, and J. I. Brand, Mater. Sci. Eng. B **135**, 129 (2006).
[4]J. Deng, Mater. Sci. Eng. A **408**, 227 (2005).
[5]H. K. Clark and J. L. Hoard, J. Am. Chem. Soc. **65**, 2115 (1943).
[6]I. Jiménez, D. G. J. Sutherland, T. van Buuren, J. A. Carlisle, L. J. Terminello, and F. J. Himpsel, Phys. Rev. B **57**, 13167 (1998).
[7]N. Vast, J. Sjakste, and E. Betranhandy, J. Phys.: Conf. Ser. **176**, 012002 (2009).
[8]Q. An, W. Goddard, and T. Cheng, Phys. Rev. Lett. **113**, 095501 (2014).
[9]B. Morosin, G. H. Kwei, A. C. Lawson, T. L. Aselage, and D. Emin, J. Alloys Compd. **226**, 121 (1995).
[10]B. Tang, Q. An, and W. A. Goddard III, J. Phys. Chem. C **119**, 24649 (2015).
[11]K. Wade, J. Chem. Soc. D **1971**, 792.
[12]M. Chen, J. W. McCauley, and K. J. Hemker, Science **299**, 1563 (2003).
[13]K. M. Reddy, P. Liu, A. Hirata, T. Fujita, and M. W. Chen, Nat. Commun. **4**, 2483 (2013).
[14]S. Zhao, B. Kad, B. A. Remington, J. C. Lasalvia, C. E. Wehrenberg, K. D. Behler, and M. A. Meyers, Proc. Natl. Acad. Sci. U.S.A. **113**, 12088 (2016).
[15]D. Gosset, S. Miro, S. Doriot, G. Victor, and V. Motte, Nucl. Instrum. Methods Phys. Res. Sect. B Beam Interact. Mater. Atoms **365**, 300 (2015).
[16]M. Chen and J. W. McCauley, J. Appl. Phys. **100**, 123517 (2006).
[17]G. Fanchini, J. W. McCauley, and M. Chhowalla, Phys. Rev. Lett. **97**, 035502 (2006).
[18]Q. An and W. A. Goddard, Phys. Rev. Lett. **115**, 105501 (2015).
[19]J. Li, S. Xu, L. Liu, Z. Wang, J. Zhang, and Q. Liu, Mater. Res. Express **5**, 055204 (2018).
[20]Q. An, W. A. Goddard, K. Y. Xie, G. D. Sim, K. J. Hemker, T. Munhollon, M. F. Toksoy, and R. A. Haber, Nano Lett. **16**, 7573 (2016).
[21]B. Tang, Y. He, W. A. Goddard, and Q. An, J. Am. Ceram. Soc. **102**, 5514 (2019).
[22]W. M. Guo, Z. L. Zhang, J. X. Li, Y. You, S. H. Wu, and H. T. Lin, Ceram. Int. **42**, 11486 (2016).
[23]K. Y. Xie, Q. An, M. F. Toksoy, J. W. McCauley, R. A. Haber, W. A. Goddard, and K. J. Hemker, Phys. Rev. Lett. **115**, 175501 (2015).
[24]K. M. Reddy, P. Liu, Y. Shen, T. Goto, Q. An, and M. W. Chen, Mater. Res. Lett. **7**, 75 (2019).
[25]H. Itoh, I. Maekawa, and H. Iwahara, J. Mater. Sci. **35**, 693 (2000).
[26]S. Xiang, L. Ma, B. Yang, Y. Dieudonne, G. M. Pharr, J. Lu, D. Yadav, C. Hwang, J. C. LaSalvia, R. A. Haber, K. J. Hemker, and K. Y. Xie, Sci. Adv. **5**, eaay0352 (2019).
[27]Q. An and W. A. Goddard, J. Phys. Chem. Lett. **5**, 4169 (2014).
[28]L. Nikzad, R. Orrù, R. Licheri, and G. Cao, J. Am. Ceram. Soc. **95**, 3463 (2012).

[29]C. Cheng, K. M. Reddy, A. Hirata, T. Fujita, and M. Chen, J. Eur. Ceram. Soc. **37**, 4514 (2017).

[30]K. Y. Xie, V. Domnich, L. Farbaniec, B. Chen, K. Kuwelkar, L. Ma, J. W. McCauley, R. A. Haber, K. T. Ramesh, M. W. Chen, and K. J. Hemker, Acta Mater. **136**, 202 (2017).

[31]K. Niihara, A. Nakashira, and T. Hirai, J. Am. Ceram. Soc. **67**, C-13 (1984).

[32]A. Chauhan, M. C. Schaefer, R. A. Haber, and K. J. Hemker, Acta Mater. **181**, 207 (2019).

[33]X. Yang, W. A. Goddard, and Q. An, J. Phys. Chem. C **122**, 2448 (2018).

[34]D. E. Taylor, J. W. McCauley, and T. W. Wright, J. Phys.: Condens. Matter **24**, 505402 (2012).

[35]D. E. Taylor, J. Am. Ceram. Soc. **98**, 3308 (2015).

[36]Y. Gu, J. X. Liu, F. Xu, and G. J. Zhang, J. Eur. Ceram. Soc. **37**, 539 (2017).

[37]L. Yang, G. Min, H. Yu, J. Han, and Y. B. Paderno, Ceram. Int. **31**, 271 (2005).

[38]L. S. Sigl, J. Eur. Ceram. Soc. **18**, 1521 (1998).

[39]K. Y. Xie, K. Kuwelkar, R. A. Haber, J. C. LaSalvia, K. J. Hemker, and R. Hay, J. Am. Ceram. Soc. **99**, 2834 (2016).

[40]D. Guo, S. Song, R. Luo, W. A. Goddard, M. Chen, K. M. Reddy, and Q. An, Phys. Rev. Lett. **121**, 145504 (2018).

[41]D. Guo and Q. An, Int. J. Plast. **121**, 218 (2019).

[42]K. D. Behler, C. J. Marvel, J. C. LaSalvia, S. D. Walck, and M. P. Harmer, Scr. Mater. **142**, 106 (2018).

[43]D. Ghosh, G. Subhash, C. H. Lee, and Y. K. Yap, Appl. Phys. Lett. **91**, 061910 (2007).

[44]D. Ge, V. Domnich, T. Juliano, E. A. Stach, and Y. Gogotsi, Acta Mater. **52**, 3921 (2004).

[45]M. N. Mirzayev, K. F. Mammadov, R. G. Garibov, and E. B. Askerov, High Temp. **56**, 374 (2018).

[46]S. Aryal, P. Rulis, and W. Y. Ching, Phys. Rev. B **84**, 184112 (2011).

[47]X. Q. Yan, Z. Tang, L. Zhang, J. J. Guo, C. Q. Jin, Y. Zhang, T. Goto, J. W. McCauley, and M. W. Chen, Phys. Rev. Lett. **102**, 075505 (2009).

[48]Q. An and W. A. Goddard, J. Phys. Chem. C **121**, 16644 (2017).

[49]S. F. Pugh, Philos. Mag. **45**, 823 (1954).

[50]A. U. Khan, A. M. Etzold, X. Yang, V. Domnich, K. Y. Xie, C. Hwang, K. D. Behler, M. Chen, Q. An, J. C. LaSalvia, K. J. Hemker, W. A. Goddard, and R. A. Haber, Acta Mater. **157**, 106 (2018).

[51]Y. He, Y. Shen, B. Tang, and Q. An, J. Am. Ceram. Soc. **103**, 2012 (2020).

[52]H. Hillebrecht, N. Vojteer, V. Sagawe, K. Hofmann, and B. Albert, Z. Anorg. Allg. Chem. **645**, 362 (2019).

[53]V. Adasch, M. Schroeder, D. Kotzott, T. Ludwig, N. Vojteer, and H. Hillebrecht, J. Am. Ceram. Soc. **132**, 13723 (2010).

[54]D. M. Teter, MRS Bull. **23**, 22 (1998).

[55]A. C. T. Van Duin, S. Dasgupta, F. Lorant, and W. A. Goddard, J. Phys. Chem. A **105**, 9396 (2001).

[56]D. Liu, K. Guo, F. Tang, F. Mao, X. Liu, C. Hou, H. Wang, H. Lu, and X. Song, Chem. Mater. **31**, 10117 (2019).

[57]R. F. K. Gunnewiek, P. M. Souto, and R. H. G. A. Kiminami, J. Nanomater. **2017**, 3983468 (2017).

[58]A. K. Khanra, Bull. Mater. Sci. **30**, 93 (2007).

[59]D. Gosset and M. Colin, J. Nucl. Mater. **183**, 161 (1991).

[60]S. V. Konovalikhin and V. I. Ponomarev, Russ. J. Inorg. Chem. **54**, 197 (2009).

[61]A. A. Cheenady, A. Awasthi, and G. Subhash, J. Am. Ceram. Soc. **103**, 7127 (2020).

[62]M. C. Schaefer and R. A. Haber, Ceramics **3**, 297 (2020).

[63]Z. Shen, R. H. Wagoner, and W. A. T. Clark, Acta Metall. **36**, 3231 (1988).

[64]H. Van Swygenhoven and P. M. Derlet, Phys. Rev. B **64**, 224105 (2001).

[65]M. W. Chen, J. W. McCauley, J. C. LaSalvia, and K. J. Hemker, J. Am. Ceram. Soc. **88**, 1935 (2005).

[66]X. Yang, S. P. Coleman, J. C. Lasalvia, W. A. Goddard, and Q. An, ACS Appl. Mater. Interfaces **10**, 5072 (2018).

[67]H. Van Swygenhoven, Science. **296**, 66 (2002).

[68]C. S. Pande and K. P. Cooper, Prog. Mater. Sci. **54**, 689 (2009).

[69]E. O. Hall, Proc. Phys. Soc. Sect. B **64**, 742 (1951).

[70]F. Liao, S. L. Girshick, W. M. Mook, W. W. Gerberich, and M. R. Zachariah, Appl. Phys. Lett. **86**, 171913 (2005).

[71]J. A. Wollmershauser, B. N. Feigelson, E. P. Gorzkowski, C. T. Ellis, R. Goswami, S. B. Qadri, J. G. Tischler, F. J. Kub, and R. K. Everett, Acta Mater. **69**, 9 (2014).

[72]X. Pang, Y. Xian, W. Wang, and P. Zhang, J. Alloys Compd. **768**, 476 (2018).

[73]M. Gao, Z. Chen, L. Li, E. Guo, Y. Kang, Y. Xu, and T. Wang, Mater. Sci. Eng. A **802**, 140453 (2021).

[74]M. Mashhadi, E. Taheri-Nassaj, V. M. Sglavo, H. Sarpoolaky, and N. Ehsani, Ceram. Int. **35**, 831 (2009).

[75]Z. Zhang, X. Du, Z. Li, W. Wang, J. Zhang, and Z. Fu, J. Eur. Ceram. Soc. **34**, 2153 (2014).

[76]L. S. Sigl and H-J Kleebe, J. Am. Ceram. Soc. **78**, 2374 (1995).

[77]H. Kim, Y.-H. Koh, and H.-E. Kim, J. Am. Ceram. Soc. **83**, 2863 (2000).

[78]X. Yan, X. Zhou, and H. Wang, Materials (Basel) **13**, 4616 (2020).

[79]A. K. Swarnakar, S. G. Huang, O. Van der Biest, and J. Vleugels, J. Alloys Compd. **499**, 200 (2010).

[80]H. W. Huang, Y. Pan, X. M. Wang, J. Yang, and K. Xu, Phys. B Condens. Matter **406**, 4539 (2011).

[81]M. Rühle, N. Claussen, and A. H. Heuer, J. Am. Ceram. Soc. **69**, 195 (1986).

[82]A. G. Evans and K. T. Faber, J. Am. Ceram. Soc. **67**, 255 (1984).

[83]D. Vallauri, I. C. Atías Adrián, and A. Chrysanthou, J. Eur. Ceram. Soc. **28**, 1697 (2008).

[84]S. Yamada, K. Hirao, Y. Yamauchi, and S. Kanzaki, J. Eur. Ceram. Soc. **23**, 1123 (2003).

[85]A. G. Evans, J. Am. Ceram. Soc. **73**, 187 (1990).

[86]Z. Krstic and V. D. Krstic, J. Mater. Sci. **47**, 535 (2012).

[87]A. Subramaniam, C. T. Koch, R. M. Cannon, and M. Rühle, Mater. Sci. Eng. A **422**, 3 (2006).

[88]X. Zhao, Q. Shu, M. C. Nguyen, Y. Wang, M. Ji, H. Xiang, K. M. Ho, X. Gong, and C. Z. Wang, J. Phys. Chem. C **118**, 9524 (2014).

[89]A. L. S. Chua, N. A. Benedek, L. Chen, M. W. Finnis, and A. P. Sutton, Nat. Mater. **9**, 418 (2010).

[90]Q. Zhu, A. Samanta, B. Li, R. E. Rudd, and T. Frolov, Nat. Commun. **9**, 467 (2018).

[91]G. Schusteritsch and C. J. Pickard, Phys. Rev. B **90**, 035424 (2014).

[92]Y. Chen, J. Chem. Phys. **130**, 134706 (2009).

[93]Y. Chen and J. Lee, Philos. Mag. **85**, 4095 (2005).

[94]L. Xiong and Y. Chen, Comput. Model. Eng. Sci. **24**, 203 (2008).